Original Article

Six-Phase Induction Motor Design and Analysis Using Wind-Driven Optimization

Saji Krishna Pillai[1], Vinod Bakka[2], J.V. Pavan Chand[3], B. Divakar[4], B.V. Sai Thrinath[5], G. Mahaboobsubahan[6]

[1,2]*Koneru Lakshmaiah Education Foundation, Vaddeswaram, Andhra Pradesh, India.*
[3]*Department of Electrical and Electronics Engineering, Lakireddy Bali Reddy College of Engineering, Andhra Pradesh, India.*
[4]*Department of Electrical and Electronics Engineering, Vignan's Institute of Information Technology, Andhra Pradesh, India.*
[5]*Department of EEE, School of Engineering, Mohan Babu University, Andhra Pradesh, India.*
[6]*Department of EEE, Annamacharya Institute of Technology and Sciences, Andhra Pradesh, India.*

[5]*Corresponding Author : connectbvst@gmail.com*

Abstract - *In this paper, a Wind-Driven Optimization (WDO) based design of a Six-Phase Induction Motor (SPIM) is presented, and it is compared to induction motors that have been traditionally designed and have the same rating. When it comes to the optimization of the design of a six-phase induction motor, a multi-objective function is taken into consideration. When compared to the conventional design motor, it has been shown that the wind-driven optimization-based optimal design yields considerably superior performance. Furthermore, the Finite Element Analyses (FEA) of every single design of a six-phase induction motor are described in this work. The purpose of this research is to determine which solution is the most cost-effective for a particular application by analyzing the performance of the motor. Additionally, in order to validate the validity of the suggested design, the quality parameters that were acquired from the WDO-based design are compared with the motor that was designed traditionally. When compared to a six-phase induction motor with ordinary control, the wind-driven optimization method for six-phase induction motors results gives a better performance like power density, efficiency, and operational power factors. With the proposed control technique, losses are mitigated by 6.7% as compared with conventional SPIM.*

Keywords - *Design optimization, Wind Driven Optimization, Six Phase Induction Motor, Finite Element Analyses, Induction generator.*

1. Introduction

To satisfy the growing need for energy, researchers have been driven further to improve the rationality of using traditional sources and examine non-traditional energy sources. The energy demand has increased due to the growing concerns over the environment and the rapid depletion of conventional energy supplies [1]. Numerous renewable energy sources, such as geothermal, wind, solar, geothermal energy, and micro-hydro, are the subjects of investigations now being carried out. Utilizing wind and hydropower is a pragmatic option to fulfil future energy demands [2].

This outcome is attributed to the abundance of instances representing both categories of generation. The ongoing study on the utilization of wind and small-scale hydropower for electricity production aims to determine the most economically efficient method of harnessing these energy sources in order to establish a reliable and high-quality power supply [3]. Induction generators are extensively utilized in micro hydro-producing systems and wind turbines due to their ability to generate efficient electricity at different speeds.

Although a generator does not produce excitation energy, it can start independently, provided specific conditions are satisfied. This is the case even though the generator does not have its generator. The speed of the rotor, the residual magnetic flux in the rotor iron, and the coupling of capacitor banks to the stator terminals are all included in these characteristics [4, 5].

During this time, the implementation of multiphase asynchronous machines was one of the ideas that was offered in order to improve the operational stability of the system. In addition, the idea of the multiphase asynchronous machine, in its whole, as well as the self-governing multiphase asynchronous generator, in particular, has been the subject of a great deal of research in the most recent years. There is no difference in the situation between these two topics [6, 7].

A six-phase induction generator can actively contribute to the self-generation of electric power across a wide range of wind speeds. This feature enables the generator to produce electrical power. This is something that can be accomplished.

One of the difficulties that may arise throughout the process of investigating self-excited generators is the task of choosing which self-priming capabilities are the most suitable.

As a consequence of this, research has been carried out in order to determine the minimum and maximum capacities for self-priming by studying the equivalent circuit of the generator in a steady state. The symmetrical components technique allows for the examination of the performance of a SPIG that supplies either in a capacitance imbalance condition or single load condition.

Additionally, the input impedance of the generator may be determined through the application of this technique. In recent years, multiphase machines have been gaining pace due to their various potential advantages over their three-phase one and their wide range of applications in high-power drives such as in industries, electric ship propulsion and traction drives [8, 9]. It is feasible to accurately evaluate the performance of the generator under a variety of load and speed situations by utilizing a numerical approach to solve a simplified equivalent circuit.

This method focuses on machine factors such as frequency and magnetizing reactance, and it is possible to evaluate the generator's performance accurately. This is made possible by the utilization of the formula. Self-excited SPIGs are gaining popularity as a means of contributing to the utilization of non-conventional energy sources like small hydro and wind. The fact that the induction generator has a tough time managing voltage when the load changes is one of the major downsides of this type of generator.

In order to ascertain the conditions under which the machine functions, stable-state analysis is a vital component. The development of algorithms that are able to forecast the performance of generators by making use of data from induction motors through computation is required in order to examine the steady-state characteristics and investigate the effects of the components. This is necessary in order to investigate the components.

Wind power generation systems have been designed using a wide variety of topologies at various points in time [10-12]. All of them are distinct from one another and come with their set of advantages and disadvantages in comparison to the others. For the purpose of achieving a high level of penetration of renewable energy into the grid, distributed generating systems are chosen over larger units that are placed at specific locations. In the event that a more extensive penetration of electricity is taken into consideration, SPIG are considered to be the most viable alternatives [13].

Compared to Doubly Fed Induction Generators (DFIG), squirrel cage Synchronous Permanent Magnet Generators (SPIG) have a number of advantages that set them apart [14].

This is due to the fact that they are less expensive and require less maintenance than DFIG. Due to the fact that squirrel cage SPIGs are more effective, this is the case. Additionally, the grid is responsible for satisfying the entire demand for reactive power resources when it is operating in grid-connected mode.

In certain situations, a capacitor might be built at the point of common connection in order to limit the amount of reactive power that is required from the grid side. This would be done in order to fulfil the requirements of the situation. In such a location, a capacitor would be installed. In situations where greater generation ratings are taken into consideration, PMSG is an excellent choice because of its large speed range and certified back-to-back converter. This makes it a perfect solution.

When SPIG is compared to PMSG, it is demonstrated that PMSG is more expensive at lower generation ratings due to the increased costs associated with its installation and operation. As a direct consequence of this finding, the payback period for PMSG is noticeably longer. This is because PMSG has a greater initial investment and a higher ongoing cost. Due to the higher costs associated with installation and operation, PMSG is the reason behind this. This is because PMSG necessitates a greater initial expenditure in addition to a higher rate of recurrent expense.

Specifically, this is the underlying factor that led to this circumstance. In light of this, fixed-speed small power generating units, also known as SPIGs, provide a viable and long-lasting alternative for smaller power sources. These units can be utilized to meet the requirements of rural areas, as well as in residential areas and small settlements.

This is a consequence of the fact that they offer a viable alternative. It is due to the fact that the cumulative output of these units has the effect of lowering the overall average grid loading that is being experienced [15, 16]. Fixed-speed SPIGs are able to generate electricity at an entirely consistent speed, which is the reason why this results in the phenomenon above [17].

Employing SPIM increases the system reliability, reduces the rotor current harmonics, and reduces the rotor copper losses and pulsating torque. Also, it has been observed that SPIM reduces stator copper losses by up to 6.7% and is less noisy as compared to its three-phase counterparts [3-5]. The availability of more phases improves the performance of SPIM during the loss of phase condition or in case of an open circuit fault [6-8].

SPIM is obtained by dividing each phase of the three-phase induction motor with a 30-degree displacement between each winding of SPIM. This paper aims to develop a new concept in the design of SPIM. WDO and simple electromagnetic equations are used for the procedure. FEA is used to validate the results.

2. Wind Driven Optimization Algorithm

It is a heuristic algorithm that takes inspiration from the flow of wind in the atmosphere of the planet, notably how it redistributes horizontal pressure. Wind Driven Optimization is an example of this inspired algorithm. The population dynamics that are described in [9] served as the foundation for the development of this optimization technique.

Airflow from regions of higher pressure to regions of lower pressure is caused by the differential air pressure and density that exists between the two places. This is due to the pressure gradient (ΔP) and is represented as,

$$\Delta P = \frac{\partial P}{\partial X}, \frac{\partial P}{\partial X}, \frac{\partial P}{\partial X} \qquad (1)$$

Newton's second rule of motion is the basis for calculating the path that an air parcel will take. This law established the framework for the calculation. According to the principle, the acceleration of an air parcel is caused by the cumulative force that is applied to it, and this acceleration takes place in the same direction as the cumulative force that is applied.

$$\rho a = \sum F_I \qquad (2)$$

Where the symbol ρ denotes the density of the air packet and the symbol a denotes the acceleration of the air packet. The collective forces affecting the air packets are referred to as FI. Four basic forces affect the trajectory and velocity of air parcels, and Equation (2) considers these forces. The pressure gradient is the primary force that causes the motion of an air parcel, and the symbol subscript base represents it since it is the force that causes the motion.

$$F_{PG} = -\Delta P. \partial V \qquad (3)$$

Where ∂V is the small volume. At the same time that the force FPG is causing movement, the frictional force acts as a counterforce to that movement.

$$F_f = -\rho. \alpha. \vartheta \qquad (4)$$

The symbol ρ is used to denote the coefficient of friction, whereas the symbol ϑ is used to represent the vector of the wind's current velocity. When air packets are subjected to gravitational force, they experience an attractive pull, which causes them to move in the direction of the centre of the rectangular coordinate system. When expressed quantitatively, this force can be described as,

$$F_V = \rho. \delta V. g \qquad (5)$$

Where g is the gravitational constant. The Coriolis force is a torque that is caused by the rotation of the earth, which in turn causes a rotation in the reference frame. This torque can be written as,

$$F_C = -2\Omega \times \vartheta, \qquad (6)$$

Where v is the earth rotation vector. The forces mentioned above are incorporated in Equation (2) and can be expressed as,

$$\rho a = -\Delta P. \partial V - \rho. \alpha. \vartheta + \rho. \delta V. g - 2\Omega \times \vartheta \qquad (7)$$

Through the utilization of the ideal gas law, we can replace the idea of density with the variables of pressure, temperature, and the universal gas constant. Alterations can be made to the Equation (7).

$$\Delta \vartheta = -\alpha. \vartheta - \Delta P \frac{RT}{P_{cur}} + g + \left(\frac{-2\Omega \times \vartheta. RT}{P_{cur}}\right) \qquad (8)$$

In this equation, the letters P, R, and T stand for pressure, the universal gas constant, and the absolute temperature, respectively. The value of the pressure exerted on a particular parcel is represented by the symbol Pcur. In the context of WDO, the velocity and position of each air parcel are continually updated after each iteration in order to aid the exploration of its search space. This is done in order to understand the search space better. It is possible to represent the change in velocity, denoted by Δv, as:

$$\Delta \vartheta = \vartheta_{new} - \vartheta \qquad (9)$$

Both the velocity and position updates that are performed by the WDO method are comparable to those that are performed by the particle-based approach. An additional degree of freedom is added to the solution space as a result of the incorporation of gravitational and Coriolis forces into the equation that is used to update the velocity of the WDO method. The flow chart of the WDO algorithm is depicted in Figure 1, which is based on the information supplied in reference.

2.1. Basic Sizing Equation

The basic sizing equation of SPIM is defined as [14],

$$S = 11K_w \times B_{av} \times q \times \left(\frac{D}{1000}\right)^2 \times \frac{L}{1000} \times n \qquad (10)$$

Where S is the rating of the motor in Watts, K_{w1} is the winding factor; B_{av} and q is the specific magnetic and electrical loading in Tesla and A/m, respectively. D and L are the stator's inner diameter and motor length in mm, respectively, and n represents the rated speed in revolutions per second. The magnetic and electric loading values are selected at the start of the design process and are restricted by the iron losses, copper losses, load profile, cooling tendency and the duty cycle.
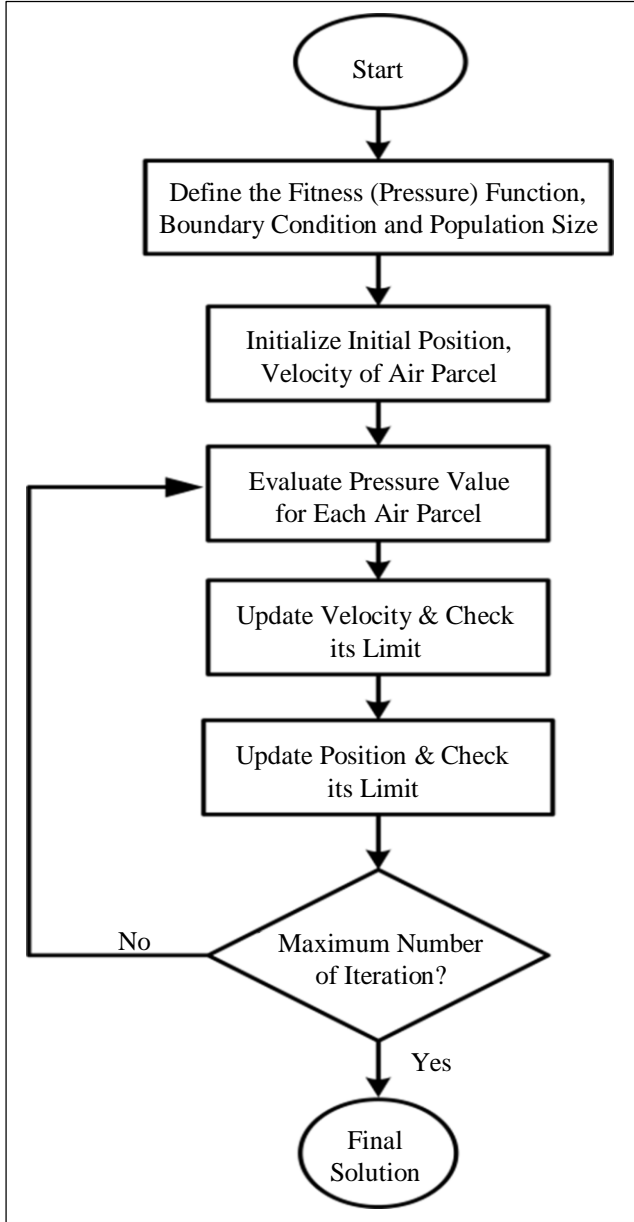
Fig. 1 Flow chart of the WDO algorithm

2.2. Aspect Ratio

The value of D2L is then determined by Equation (1). Aspect ratio λ is also a design parameter, and its value should be primarily selected at the beginning of the design process so that D and L can be determined. For a p-pole machine with a shorter length, an appropriate value of λ increases the induced emf in the winding as it is proportional to the coil area for the same flux density,

$$\lambda = \frac{L}{\pi \frac{D}{P}} = \frac{L}{Y} \tag{11}$$

Where y is the peripheral distance between the two poles in meters.

2.3. Selection of Current Density

Following the selection of the required values for the average magnetic field strength Bav, charge q, and wavelength λ, the current density Js that corresponds to a particular rated current I is utilized in order to compute the cross-sectional area Ac of the copper wire.

$$A_s = \frac{I}{J_s} \tag{12}$$

A smaller cross-section area leads to higher armature resistance and greater current density as a result of increased copper losses, which lower the motor's efficiency. So, in conventional design, the current density value is selected in the range of 3-7A/mm2 depending on the designer's experience or by thumb rule [11, 12].

2.4. Flux Density

The flux density in the core and teeth is selected at the vicinity of the knee point of the B-H curve in such a way that it fully utilizes the material. For silicon steel based design, a point of flux density is near 1.5T [11].

2.5. Design Process of SPIM

An electrical machine design is a rigorous iterative process, as shown in Figure 1, with an appropriate assumption of power factor and efficiency to determine the rating of machine S in volt-amp.

$$\text{Maching rating(S)} = \frac{\text{Output power}(P_{out})}{\eta \times \text{Power factor}} \tag{13}$$

Wire diameter and number of turns of the stator coils at a specified current density and voltage for a given winding layout are then determined. By selecting flux density in the core and teeth, the thickness of the core and tooth width is calculated. The outer diameter of the machine is then calculated from the area of the core and teeth and by the slot area of the winding. The design of the rotor is also done with some empirical rules [11].

After completion of the design, a performance check of the obtained design is done, and the parameters' values are compared with the reference parameters. Suppose the parameters do not meet the specifications of the motor. In that case, some modification has to be done to meet the requirement, and the whole design process is repeated as many times until the parameters meet the specified values.

2.6. 2-Dimension Eddy-Current Model of SPIM

Eddy-current model of SPIM in 2-Dimension is defined by using the sets of Maxwell equations and is represented by the equation as follows [13]:

$$\frac{\partial}{\partial x}\left(v\frac{\partial A}{\partial x}\right) + \frac{\partial}{\partial y}\left(\frac{\partial A}{\partial y}\right) = -J + \sigma\frac{\partial A}{\partial t} \tag{14}$$

Where σ is the material's conductivity, the magnetic field and source will change sinusoidally with time for the linear model. Hence, J and A are sinusoidal vectors, and ∂A/∂t can be represented by jωA. Also,

$$W(A) = \iint \left[\int_0^B H dB - JA + \frac{1}{2} J\omega\sigma A^2 \right] d\Omega + \iint H_t \, Ads = \min \tag{15}$$

B is the magnetic flux density, and H is the magnetic field strength [13].

3. Objective Functional Constraints

It has been written and successfully tested in SPIM that the design program for the application that was specified in MATLAB has been written. After that, the values of the SPIM parameters were evaluated and checked for accuracy while simultaneously ensuring that they complied with the limits. Using the sources [11, 14], the design program of SPIM is produced during the development process. For design optimization of SPIM, the selection of the objective function is contingent upon the performance objectives, and it is necessary to give significant consideration to this matter. Figure 2 is an illustration of the flow chart that depicts the SPIM when using the traditional approach. Following that, the formulation takes into consideration a function that has many objectives [14]: To minimize the stator copper loss.

$$P_{CU(Stator)} = 6 \times I_{ph}^2 \times R_s \tag{16}$$

Where I_{ph} = phase current in Amperes and R_S = stator resistance in Ohm.

3.1. Minimization of the Rotor Copper Losses

$$P_{CU(Rotor)} = \frac{r_r \times S_2 \times I_b^2}{a_a} \left(1 + \frac{2 \times D_e}{P}\right) \tag{17}$$

The variables in the equation are as follows: rr is a constant with a value of 0.021, S2 represents the number of rotor slots, Ib represents the rotor bar current in amperes, De represents the mean diameter of the end ring in millimetres, Lr represents the core length in meters, and P represents the number of poles.
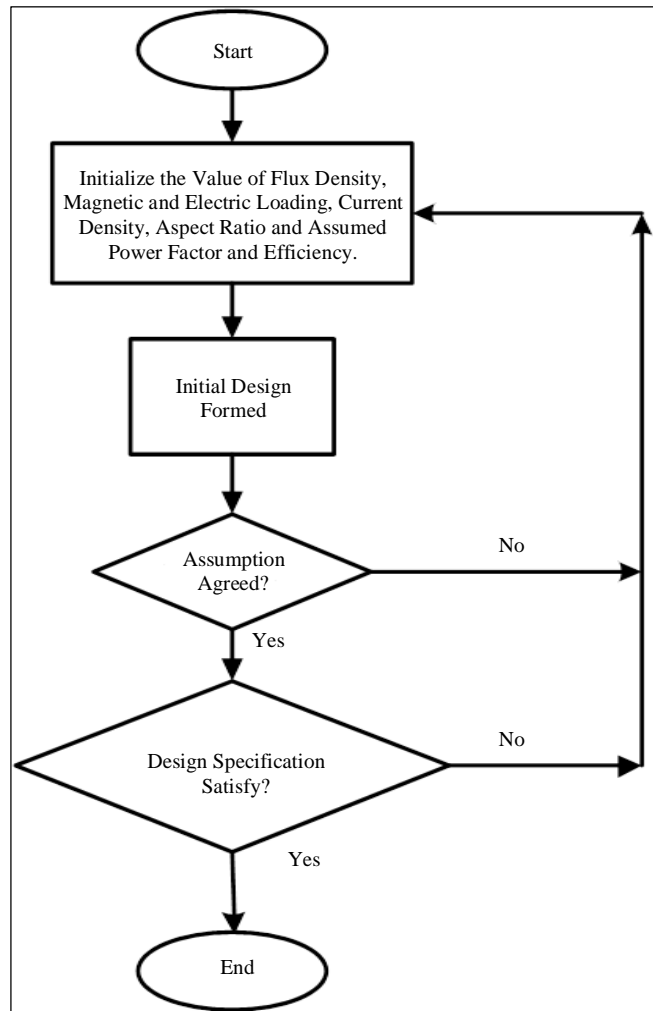

Fig. 2 Flow chart of SPIM design by traditional method

3.2. Minimization of the Stator Iron Losses

$$P_{I(Stator)} = W_t \times W_{tk} + W_c \times W_{ck} \qquad (18)$$

Where Wt represents the weight of the stator teeth, Wc represents the weight of the stator core, Wtk represents the stator tooth losses in terms of W per kilogram, and Wck represents the stator core losses in terms of W per kilogram.

3.3. Full Load Efficiency

$$\eta = \frac{1000 \times P_0}{1000 \times P_0 + P_{CU(Stator)} + P_{CU(Rotor)} + P_{I(Stator)} + P_{Friction}} \qquad (19)$$

Where P_o = power in KW, $P_{Friction}$ = friction losses in kW.

The optimisation process is subject to constraints such as starting current and starting torque in order to facilitate the achievement of a level of performance that is deemed sufficiently adequate. Figure 3 depicts the five parameters that are chosen to be the primary motor variables in the optimization process. These parameters are the focus of the optimization process. Several variables are of interest, including the following: the length of the stator core (x1), the depth of the stator slot (x2), the width of the stator teeth (x3), the inner diameter of the stator (x4), the depth of the stator core (x5), and the power factor (x6). For optimization, the motor that possesses the ratings that were specified, as shown in Table 1, has been chosen. The sample time used here is 50µS, so 20k samples are generated in one sec.
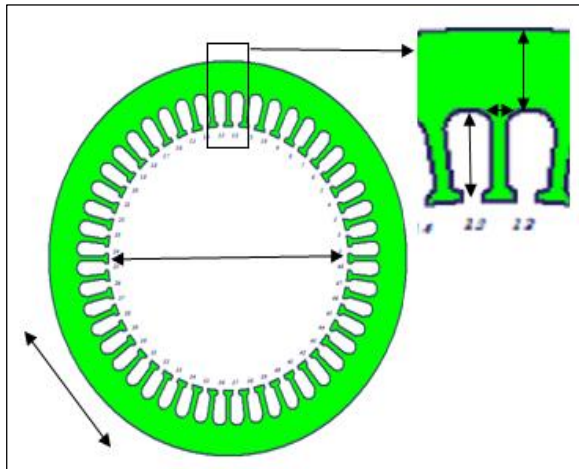

Fig. 3 Stator optimization parameters

Table 1. Parameters of SPIM

Phase Number	6	Power Rating (KW)	1.1
Rated Phase Voltage(v)	400	Stator Slot Number	48
Connection	Y	Supply Frequency (in Hz)	50
Rotor Slot Number	38	Poles Number	4

4. Results and Analysis

Presented in the form of a flow chart, Figure 3 illustrates the design optimization technique that was established not too long ago. Each block contains a significant number of subroutines that are contained within it. Before commencing the execution of the program, it is necessary to take into mind the performance parameters. This is a crucial step that must be taken.

There are a number of important features of the initial motor design that are incorporated into the parameters. These include the number of generations, the size of the population, the rate of crossover, and the rate of mutation. There are a lot of configurable settings available to the user, including the number of generations, the crossover rate, and the mutation rate.

The user can choose these options according to their tastes. It is conceivable for these parameters and functions to undergo small modifications if the values of each design parameter and the limits of each penalty function are within the bounds of their respective domains. This is the case if the design parameters and functions are in a state of equilibrium. The use of computers is employed for the purpose of computing the design parameters that are responsible for determining the arrangement of the stator and rotor together.

The power factor must be at least 0.79 in order to satisfy the requirements given. That the initial current might be greater than 7.5 (per unit) is a possibility that should not be discounted. Beginning torque must be present at a minimum of two (per unit) in order to be considered present. It is recommended that the stator, rotor core, and teeth of the rotor have a flux density that is approximately 1.5 times higher than the maximum flux density.

The constraints that have been provided determine the boundaries of the optimization technique in a very specific manner. When there is no load, it is advised that the power factor is between 0.15 and 0.28. This is done in order to obtain the highest potential level of performance within the system. The characteristics of the WDO program are described in Table 2, and a summary of the outcomes that were accomplished as a result of using the improved WDO SPIM design is presented in Table 3. Both tables may be found below. Figure 4 provides a visual representation of the motor design that was built with the assistance of ANSYS.

Table 2. Control parameters for WDO

Population Size	20	Number of Input Samples	100	Iteration Cycles	500
Constant, RT	3	Coriolis Effect	0.4	Gravitational Constant	0.2

Table 3. Comparison of output summary obtain from traditional method and WDO

Quantity	Traditional Method	WDO
Power Factor (PF)	0.85	0.89
Efficiency(η)	0.8032	0.829946
Total Losses	149.2948	123.928
No Load Power Factor	0.1180	0.1832
Stator Resistance (Ω)	8.7723	16.3815
Equivalent Resistance (Ω)	15.3132	54.2473
Equivalent Reactance (Ω)	34.0914	17.4236
Reactance Magnetizing(Ω)	379.50	250
Length of Stator Stack (m)	0.0481	0.0675
Inner Stator Diameter (m)	0.1041	0.0696
Inner Rotor Diameter (m)	0.0512	0.019
Stator Teeth Width (m)	0.0020	7 0.006
Stator Slot Depth (m)	0.0171	0.011
Width of Stator Slot (m)	0.0088	1 0.0111
Stator Core Depth (m)	0.0067	0.0128125
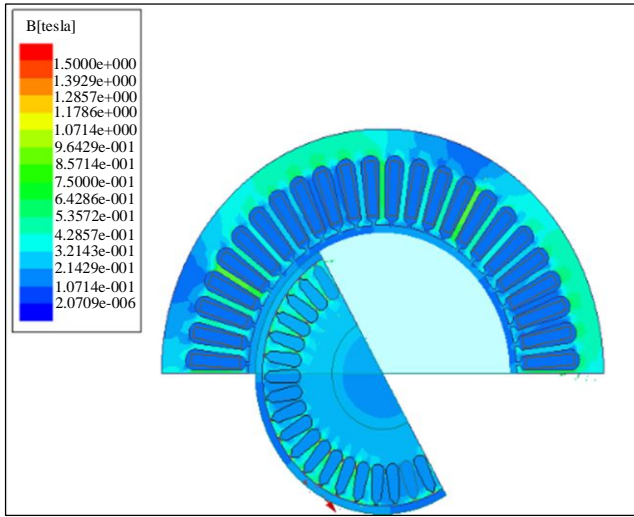
When compared to the conventional design, the optimal design leads to a reduction of losses of up to five per cent and an increase in efficiency of about five per cent than the traditional design.

The machine's working power factor also improved to about 0.9 lag, which is a significant improvement. The characteristics that are acquired from a design that is based on WDO and has phase voltage, on the other hand, are lower when compared to the characteristics that are achieved from a traditional design.

Because the motor has a power output of 1000 W, which is substantially closer to that of the typical motor, the fact that there is almost no mistake in the output power proves that the WDO-based design is correct. The losses are mitigated by 6.7% as compared to conventional SPIM.

This is because the manufactured motor has a power output that is significantly like that of the normal motor. Furthermore, the flux density that is computed using FEA is in good agreement with the value that is acquired through the use of traditional design.

5. Conclusion

This paper presents the design optimization of a six-phase induction motor that was accomplished through the utilization of WDO. For optimization, quality measures such as power factor, losses, and efficiency were taken into consideration.

References

[1] Chih-Hong Lin, and Chang-Chou Hwang, "Multiobjective Optimization Design for a Six-Phase Copper Rotor Induction Motor Mounted with a Scroll Compressor," *IEEE Transactions on Magnetics*, vol. 52, no. 7, pp. 1-4, 2016. [CrossRef] [Google Scholar] [Publisher Link]

[2] Mohana Kishore Pinjala, and Ravikumar Bhimasingu, "Improving the DC-Link Utilization of Nine-Switch Boost Inverter Suitable for Six-Phase Induction Motor," *IEEE Transactions on Transportation Electrification*, vol. 6, no. 3, pp. 1177-1187, 2020. [CrossRef] [Google Scholar] [Publisher Link]

[3] Asghar Taheri, Abdolreza Rahmati, and Shahriyar Kaboli, "Efficiency Improvement in DTC of Six-Phase Induction Machine by Adaptive Gradient Descent of Flux," *IEEE Transactions on Power Electronics*, vol. 27, no. 3, pp. 1552-1562, 2012. [CrossRef] [Google Scholar] [Publisher Link]

[4] Tiejun Wang et al., "Novel Filter for Stator Harmonic Currents Reduction in Six-Step Converter Fed Multiphase Induction Motor Drives," *IEEE Transactions on Power Electronics*, vol. 28, no. 1, pp. 498-506, 2013. [CrossRef] [Google Scholar] [Publisher Link]

[5] Ghasem Rezazadeh et al., "Improved Design of an Outer Rotor Six-Phase Induction Motor with Variable Turn Pseudo-Concentrated Windings," *IEEE Transactions on Energy Conversion*, vol. 37, no. 2, pp. 1020-1029, 2022. [CrossRef] [Google Scholar] [Publisher Link]

[6] Khaled Laadjal et al., "Online Diagnosis and Discrimination of Stator Faults in Six-Phase Induction Motors Based on Voltage Symmetrical Components," *IEEE Transactions on Transportation Electrification*, vol. 9, no. 2, pp. 3115-3126, 2023. [CrossRef] [Google Scholar] [Publisher Link]

[7] Mohammad Hosein Holakooie, Mansour Ojaghi, and Asghar Taheri, "Direct Torque Control of Six-Phase Induction Motor with a Novel MRAS-Based Stator Resistance Estimator," *IEEE Transactions on Industrial Electronics*, vol. 65, no. 10, pp. 7685-7696, 2018. [CrossRef] [Google Scholar] [Publisher Link]

[8] Viju Nair R. et al., "Novel Symmetric Six-Phase Induction Motor Drive Using Stacked Multilevel Inverters with a Single DC Link and Neutral Point Voltage Balancing," *IEEE Transactions on Industrial Electronics*, vol. 64, no. 4, pp. 2663-2670, 2017. [CrossRef] [Google Scholar] [Publisher Link]

[9] Asghar Taheri, Hai-Peng Ren, and Mohammad Hosein Holakooie, "Sensorless Loss Model Control of the Six-Phase Induction Motor in All Speed Range by Extended Kalman Filter," *IEEE Access*, vol. 8, pp. 118741-118750, 2020. [CrossRef] [Google Scholar] [Publisher Link]

[10] Shaikh Mohammed Suhel, and Rakesh Maurya, "A New Switching Sequences of SVPWM for Six-Phase Induction Motor with Features of Reduced Switching Losses," *CES Transactions on Electrical Machines and Systems*, vol. 5, no. 2, pp. 100-107, 2021. [CrossRef] [Google Scholar] [Publisher Link]

[11] Emerson L. Soares et al., "A Multilevel Open-End Winding Six-Phase Induction Motor Drive Topology Based on Three Two-Level Three-Phase Inverters," *IEEE Transactions on Industry Applications*, vol. 59, no. 5, pp. 6360-6372, 2023. [CrossRef] [Google Scholar] [Publisher Link]

[12] Sudheer Adigintla, Mohan V. Aware, and N. Arun, "Fractional Order Transfer Function Identification of Six-Phase Induction Motor Using Dual-Chirp Signal," *IEEE Journal of Emerging and Selected Topics in Power Electronics*, vol. 11, no. 5, pp. 5183-5194, 2023. [CrossRef] [Google Scholar] [Publisher Link]

[13] Jay K. Pandit et al., "Direct Torque Control Scheme for a Six-Phase Induction Motor with Reduced Torque Ripple," *IEEE Transactions on Power Electronics*, vol. 32, no. 9, pp. 7118-7129, 2017. [CrossRef] [Google Scholar] [Publisher Link]

[14] R. Viju Nair, and K. Gopakumar, "Novel Method for Instantaneous Neutral Point Voltage Balancing for a Stacked Multilevel Inverter-Fed Six-Phase Induction Motor Drives," *IEEE Journal of Emerging and Selected Topics in Power Electronics*, vol. 10, no. 6, pp. 6910-6917, 2022. [CrossRef] [Google Scholar] [Publisher Link]

[15] Mahmoud M. Amin et al., "MRAS-Based Super-Twisting Sliding-Mode Estimator Combined with Block Control and DTC of Six-Phase Induction Motor for Ship Propulsion Application," *IEEE Transactions on Industry Applications*, vol. 57, no. 6, pp. 6646-6658, 2021. [CrossRef] [Google Scholar] [Publisher Link]

[16] Sayan Paul, and Kaushik Basu, "A Three-Phase Inverter Based Overmodulation Strategy of Asymmetrical Six-Phase Induction Machine," *IEEE Transactions on Power Electronics*, vol. 36, no. 5, pp. 5802-5817, 2021. [CrossRef] [Google Scholar] [Publisher Link]

[17] Hamza Mesai-Ahmed et al., "Multiple Open-Circuit Faults Diagnosis in Six-Phase Induction Motor Drives Using Stator Current Analysis," *IEEE Transactions on Power Electronics*, vol. 37, no. 6, pp. 7275-7285, 2022. [CrossRef] [Google Scholar] [Publisher Link]